Journal of
Synchrotron
Radiation

ISSN 1600-5775

Received 6 August 2014
Accepted 2 October 2014

Large-acceptance diamond planar refractive lenses manufactured by laser cutting

Maxim Polikarpov,[a,b] Irina Snigireva,[b] John Morse,[b] Vyacheslav Yunkin,[c] Sergey Kuznetsov[c] and Anatoly Snigirev[b]*

[a]Immanuel Kant Baltic Federal University, Nevskogo 14a, 23600 Kaliningrad, Russian Federation, [b]European Synchrotron Radiation Facility, 71 avenue des Martyrs, Grenoble 38043, France, and [c]Institute of Microelectronics Technology RAS, Chernogolovka 142432, Russian Federation. *E-mail: snigirev@esrf.fr

For the first time, single-crystal diamond planar refractive lenses have been fabricated by laser micromachining in 300 μm-thick diamond plates which were grown by chemical vapour deposition. Linear lenses with apertures up to 1 mm and parabola apex radii up to 500 μm were manufactured and tested at the ESRF ID06 beamline. The large acceptance of these lenses allows them to be used as beam-conditioning elements. Owing to the unsurpassed thermal properties of single-crystal diamond, these lenses should be suitable to withstand the extreme flux densities expected at the planned fourth-generation X-ray sources.

Keywords: X-ray optics; refractive lenses; diamond planar lenses; beam conditioning; diamond processing; laser micromachining.

1. Introduction

Since the end of the 20th century, the intensive development of X-ray refractive optics instrumentation and tools has given birth to X-ray refractive lenses (Snigirev *et al.*, 1996; Lengeler *et al.*, 1999; Shabel'nikov *et al.*, 2002; Schroer & Lengeler, 2005; Snigirev *et al.*, 2009) which have proven to be compact, in-line, stable, easily aligned, and coherence-preserving for micro- and nano-beam focusing applications on third-generation synchrotron radiation sources. Over half the beamlines at the European Synchrotron Radiation Facility now employ refractive lenses as beam-shaping and beam-conditioning optics, including new monochromatization (Vaughan *et al.*, 2011) and harmonic rejection schemes (Polikarpov *et al.*, 2014). In view of the global trend towards the development of ultimate storage rings, and in particular the proposed ESRF machine 'Phase II' upgrade programme, there is a growing need for 'front-end' beam-conditioning optics to reduce beam divergence and size prior to its downstream beamline propagation. This requires X-ray optics fabricated from materials that can withstand extreme heat and radiation loads while still providing effective focusing. Diamond, as will be shown in the following paragraph, can satisfy all the requirements provided that a suitable lens-manufacturing technology is available.

The refractive index n of a material may be described by the formula $n = 1 - \delta + i\beta$, where the refractive index decrement δ is associated with the phase shift of the X-ray beam (*i.e.* the material's ability to refract X-rays), and β is associated with the X-ray absorption in the lens material (in other words β characterizes the transparency of the lens). For a beam traversing a slab of the material, δ/β is the ratio of the phase shift that occurs to the loss of intensity (Tummler, 2000). Better optical performance is obtained in materials with high values of δ/β, and for typical synchrotron hard X-ray energies such as, for example, 10 keV, the δ/β ratio of 1000 in diamond is reasonably high and not far below that of beryllium (4000) which is currently the most widely used material for the manufacture of X-ray refractive lenses. However, the value of δ in diamond is twice that of beryllium so that, for the same lens geometry, two times fewer diamond lenses are required to achieve the same focal distance in the experimental setup (in accordance with the formula $F = R/2N\delta$, where F is the focal distance and N is the number of lenses). In addition, diamond is an attractive choice of material for use in white- or pink-beam applications due to its high thermal conductivity (κ), low thermal-expansion coefficient (α), high temperature stability and chemical inertness. Materials can be thermo-mechanically ranked by the figure-of-merit (κ/α) (Khounsary *et al.*, 1992; Fernandez *et al.*, 1997). At room temperature, κ/α for diamond is $\sim$100 times better than that of beryllium. This high figure-of-merit of diamond dramatically reduces the deleterious effects of heating due to absorption in white beams, so we anticipate a widespread future application of diamond for X-ray free-electron lasers and upgraded third-generation synchrotrons. A detailed summary of the relevant heat-load properties of diamond lenses can be found by Snigirev *et al.* (2002), while diamond plates are already in use for high-heat-load monochromators (Khounsary *et al.*, 1992), at synchrotron

undulator beamlines (Yabashi *et al.*, 2007; Grübel *et al.*, 1996; Fernandez *et al.*, 1997; Als-Nielsen *et al.*, 1994) and at X-ray free-electron lasers (Shu *et al.*, 2013; Stoupin *et al.*, 2013, 2014).

Despite all the benefits offered by diamond as the refractive lens material of choice, a stumbling block to its immediate use is its difficult processing: diamond presents a substantial challenge as it is both the hardest material of the periodic system and extremely chemically inert. Over the last decade, several attempts have been made by different groups to fabricate diamond planar lenses for nano-focusing purposes, mainly using polycrystalline diamond. The first planar diamond lenses (Snigirev *et al.*, 2002) were made by a transfer moulding technique (Bjiorkman *et al.*, 1999; Ralchenko *et al.*, 1999), and these were followed by kinoform planar refractive lenses (Nöhammer *et al.*, 2003) fabricated by electron-beam lithography and reactive-ion etching (RIE). The desired focusing performance was not achieved due to the low quality of the lenses that resulted from both fabrication methods: scattering occurred due to distortions, roughness of the lens surface, deviations from the ideal shape of the lens, and faceting caused by the RIE process. In addition, these planar lenses could only be manufactured with very modest depth, *e.g.* 40 μm (Nöhammer *et al.*, 2003). Subsequent attempts to improve the quality of the diamond lens (Isakovic *et al.*, 2009; Fox *et al.*, 2014) were more promising. Lenses manufactured by the transfer moulding technique (Malik *et al.*, 2013) with polycrystalline diamond (Fox *et al.*, 2014) showed an improved quality and uniformity, reaching focal line-widths down to 210 nm for an 11 keV beam energy. However, the maximum lens thickness in this case was ∼30 μm, which is far less than is required: consider the horizontal source divergence of the future-generation synchrotrons (such as the upgraded ESRF) which is ∼10 μrad, with the distance from the source to first beamline optics of ∼30 m, so for a planar lens to accept all of the beam it must have a depth of at least ∼300 μm. In addition, the optical performance of polycrystalline diamond lenses, made by moulding techniques, is inevitably limited by the strong diffuse X-ray scattering resulting from the randomly oriented diamond crystal grains formed as the polycrystalline diamond plate is grown, the slope and the roughness of the etched side walls of the 'mould' and, under certain conditions, the possibility that diamond is transformed to other forms of diamond during etching instead of being fully removed from the surface (Bello *et al.*, 2000). It should also be noted that small (1–10 μm) grain-size polycrystalline diamond, and in particular the nanocrystalline diamond which is present at the initial diamond–mould growth interface, have thermal conductivities that are a fraction of that of single-crystal material due to phonon scattering at grain boundaries and (in the case of nano-material) the presence of a high proportion of sp^2-bonded (*i.e.* graphitic) carbon.

Here we recall that a major factor in the choice of diamond as an X-ray lens material is its excellent thermal properties, which is not the most important consideration in nano-focusing applications. Because of the present poorly developed technology available for diamond micro-fabrication, diamond planar refractive nano-lenses are unable to compete in quality and focus resolution with their silicon counterparts. Accordingly, we are at present concentrating our efforts on single-crystal diamond lenses for beam-conditioning optics, as here a large lens depth and homogeneous material are essential while some non-ideality in the lens surfaces may be accepted. For this, a laser-cutting approach appears to be very promising. First attempts were made using glassy carbon material (Artemiev *et al.*, 2006), where the lenses were manufactured by direct surface evaporation using laser beam heating. With this method the available lens depth increased dramatically to 1000 μm, but further work on smoothing the laser-cut lens profiles was required. Nevertheless, with the improvement of laser machining techniques since 2006, and especially with the introduction of femtosecond laser micro-machining, it has become possible to produce lenses in diamond with a qualitatively new low level of surface micro-roughness. Here we report on planar compound refractive lenses produced by laser cutting of single-crystal diamond.

2. Lens fabrication

The lenses were fabricated using commercially available single-crystal diamond plates of size 3 mm × 3mm. These plates were grown by chemical vapor deposition (CVD) and supplied by Element Six Ltd (Ascot, UK; product reference No. 145-500-0248). Parabolic lens profiles were machined by MicroUsinage Laser (Grattentour, France; http://www.micro-usinage-laser.com/) using a tripled Nd-YAG laser (355 nm) with a combination of precision galvo-mirror beam steering and translation of the diamond support stage. Graphitic debris formed by absorption of the focused laser beam is usually cleared using a high-pressure nitrogen gas jet, although for the lenses described here this technique was not used. Remaining graphitic plumes were removed from the diamond by hot mineral acid cleaning.

Two compound refractive lenses (CRLs) (Snigirev *et al.*, 1996) with variable numbers of single lenses in a row were laser machined in the diamond plate (Fig. 1). The focal distance for both these CRLs was 13 m at an X-ray energy of 12.4 keV. One row (CRL_2) consisted of two single lenses with radius of the parabola apex of 200 μm; the second row (CRL_5) consisted of five single lenses with radius of parabola 500 μm. The geometrical aperture of both CRLs was 1 mm, while the depth of the structures was equal to the diamond plate thickness of 300 μm. The thickness of the diamond between the apexes of successive parabolas was 75 μm. This figure could be substantially reduced, but in these first fabrication tests a conservative value was used to ensure no breakage of the lenses during handling. Crossed-polarizer imaging of the processed diamond plate showed no evidence of stress resulting from the laser cutting of the lens profiles. The scanning electron micrograph (SEM) (Fig. 1) shows good quality of the lens side walls, although some 'scallop'-like roughening of the surface can be seen at the parabola apex: this roughening clearly resulted from the combination of the laser pulsing and guidance during the cutting process.

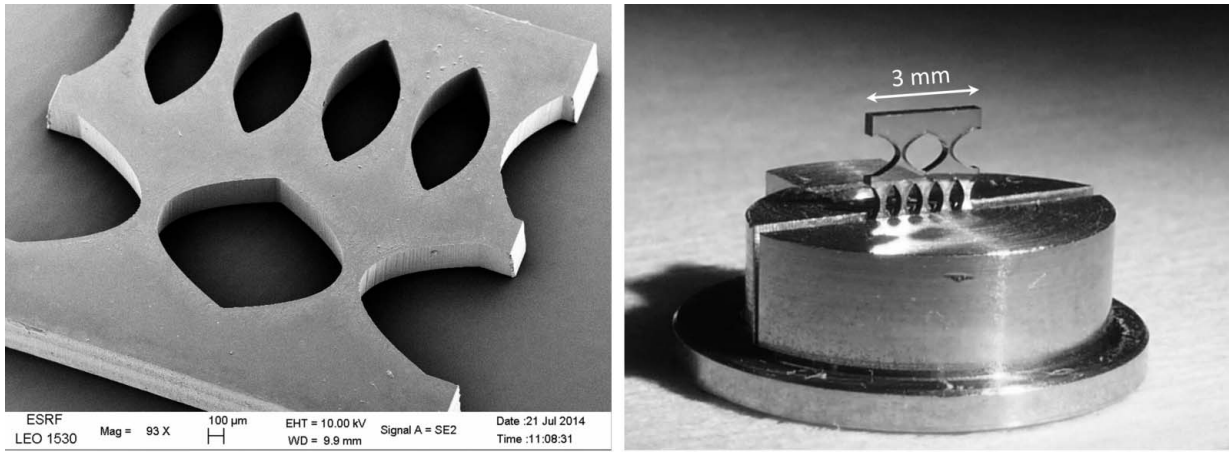

Figure 1
(Left) SEM of the diamond lens, produced by laser-cut technology, and (right) the lens mechanically clamped in a holder for the X-ray beamline tests.

3. Measurements

The diamond planar CRLs were tested at the Micro Optics Test Bench (Snigirev *et al.*, 2007) at the ID06 beamline of the ESRF. The beam was produced by an in-vacuum undulator and desired X-ray energies selected by a cryogenically cooled Si (111) double-crystal monochromator. The vertical and horizontal source sizes were 40 µm and 900 µm (full width at half-maximum, FWHM), respectively. The diamond CRLs were located at $L_1 = 55$ m from the undulator source and were mounted on motorized stages enabling all necessary translation and rotation alignments. The lenses were oriented so as to focus in the vertical direction, and an upstream vertical slit size adjusted to avoid radiation impinging on the lenses outside their effective aperture (Kohn *et al.*, 2003). The size of the horizontal slit used corresponded to the depth (300 µm) of the diamond plate. Two sets of diamond CRLs were tested, named SET#1 and SET#2; these had nominally identical geometries, but SEM images of the lens arrays showed some slight variation in the roughness of their profiles resulting from variations in the laser processing. The measurements of the CRL efficiencies and sizes of the focal lines were performed using a high-resolution X-ray CCD camera (0.64 µm pixel size), while the CRL's effective apertures were measured by scanning a 10 µm-wide vertical slit through the image plane of the lenses while recording the beam intensity with a silicon pin-diode. The layout of the experiment is shown in Fig. 2.

The measurements of the width of the focal line in the vertical direction (FWHM) and the intensity gain were performed at the energy range from 7 to 12 keV. The results of the measurements conducted at 10.3 keV for both lens arrays CRL_2 and CRL_5 of the two CRL sets are presented in Table 1. The image distance L_2 was ~8.3 m; therefore a source demagnification factor of 6.6 was achieved, while the effective aperture $A_{\rm eff}$ of both CRLs was 650 µm at this energy. The focal spot obtained with the CRL SET#2 was slightly worse than that of SET#1, and this correlated with the slightly rougher surface profiles observed in the SEM images for SET#2. Fig. 3 shows the focusing by the CRL_2 SET#1. The vertical size of the image is 5.7 µm (FWHM), which corresponds to an X-ray effective source size of 40 µm measured using the boron fibre interferometer technique (Kohn *et al.*, 2000). The focal depth was of the order of a few centimetres. As expected, the intensity gain for CRL_5 was lower than that of CRL_2 as CRL_5 has more individual lenses.

The uniform intensity of the images of the focused beam shows the high quality of the lens side walls, *i.e.* their uniform verticality. Unfortunately, the measured gain of 35 is almost one half of that of the calculated value: we attribute this to undesirable scattering resulting from the 'scallop'-like

Table 1
Experimental results at energy 10.3 keV.

CRL	Set number	FWHM (µm)	Gain (calculated)	Gain (measured)
CRL_2: $N = 2$ lenses with $R = 200$ µm	SET#1	5.7	73	35
	SET#2	6.3	73	34
CRL_5: $N = 5$ lenses with $R = 500$ µm	SET#1	6.2	46	23
	SET#2	7.6	46	22

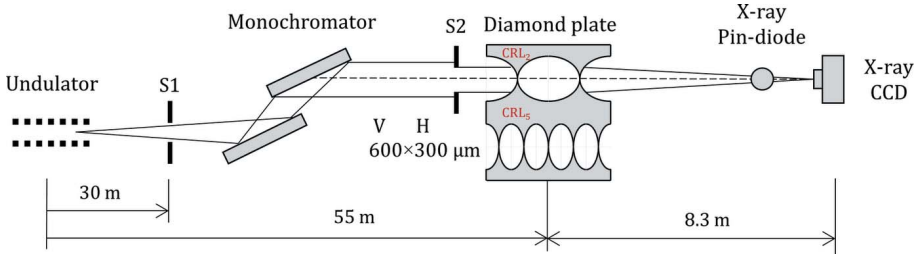

Figure 2
Layout for the ID06 beamline measurements.

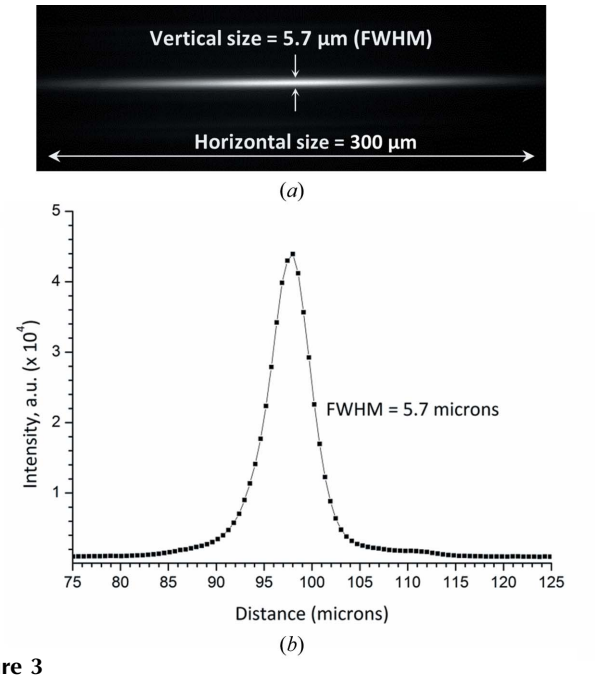

Figure 3
(*a*) X-ray image of the focal line produced by CRL_2 (two single lenses) SET#1. The horizontal size of the image is 300 μm, which corresponds to the relief depth of the diamond plate. (*b*) Measured profile of the focused X-ray beam at 10.3 keV. The vertical width of the focal line is 5.7 μm (FWHM), which almost corresponds to the initial source size 40 μm.

roughness of the lens surfaces. As the laser is pulsed and its beam movement is not fully continuous, larger amounts of the material evaporate at the stop points, producing the scalloped lens profile.

Let us consider this roughness as a sine-modulated deviation $d(x)$ from the ideal parabolic profile in the direction which is normal to the lens' surface. In this case

$$d(x) = d_0 \sin\left[2\pi \frac{L(x)}{T}\right], \quad (1)$$

where d_0 is the magnitude of the deviation, $L(x)$ is the arc length of the parabola; T is the period of the deviation and x is the coordinate across the optical axis. The arc length of the parabola with radius of curvature at the parabola apex R is

$$L(x) = \frac{R}{2}\left\{\frac{x}{R}\left(1+\frac{x^2}{R^2}\right)^{1/2} + \ln\left[\frac{x}{R}+\left(1+\frac{x^2}{R^2}\right)^{1/2}\right]\right\}. \quad (2)$$

Fig. 4(*a*) shows the sine-modulated profile with the magnitude of d_0 = 1 μm and the period of T = 22 μm together with the ideal parabolic lens profile. The calculated intensity distributions along and across the optical axis for focusing by an ideal and the distorted (d_0 = 1 μm) lens profiles are shown in Figs. 4(*b*) and 4(*c*). These figures are only an illustration of the influence of the lens profile on the focusing quality, as we assumed here a plane wave from a point source which has been focused by two single lenses of radius R = 200 μm in the same geometry as for the real experiment. However, even this slightly simplified modelling shows that the presence of the described deviation d has a strong negative influence on the optical properties of the lenses in terms of the focal line width

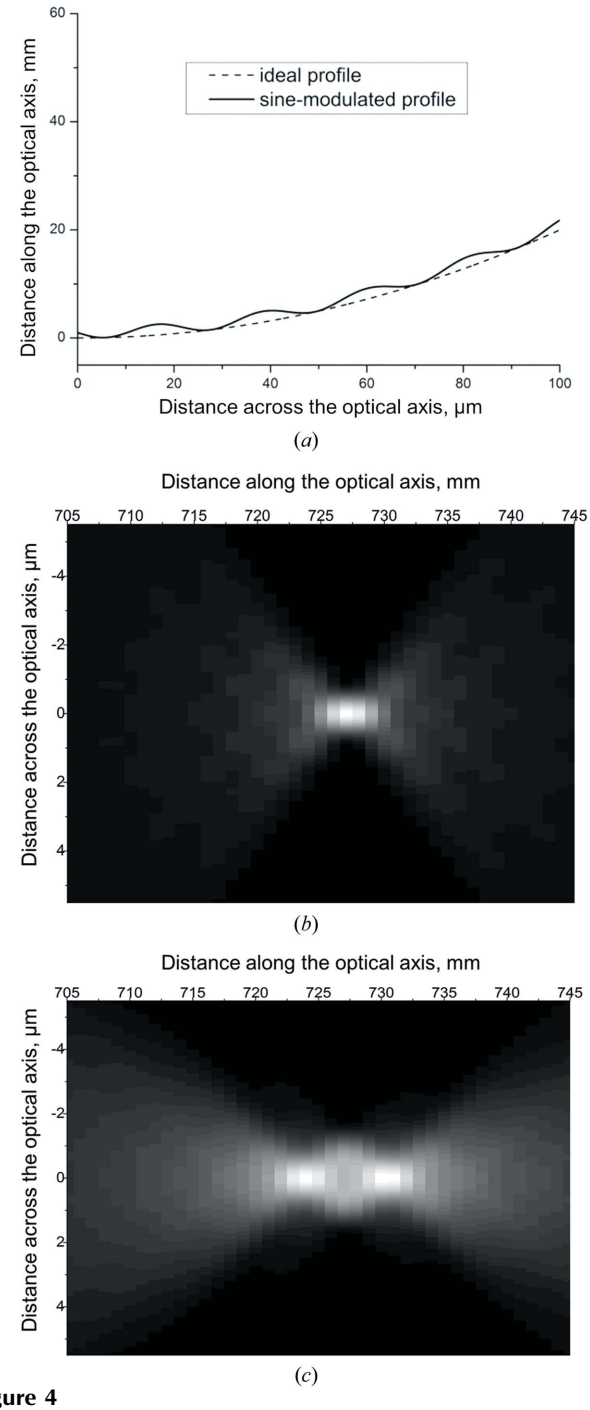

Figure 4
(*a*) Calculated ideal parabolic and sine-modulated (d_0 = 1 μm) lens profiles. Theoretical intensity distributions along and across the optical axis for focusing by (*b*) an ideal and (*c*) the distorted (d_0 = 1 μm) lens profiles.

and gain: the width of the focal line is much broader and with less intensity for the deviated profile, and the focal depth is much sharper for the lens with the ideal profile. The effect is more pronounced if d is greater than 0.5% of the lens radius or, in other words, the negative influence is stronger for lenses with a small radius of curvature of the parabola apex R. Returning to our experimental results, taking a roughness value of $2d_0$ = 2.5 μm, consistent with the SEM images of the

lens apexes, the theoretical gain calculations are very close to those obtained experimentally.

Two-dimensional focusing was also realised by placing SET#1 and SET#2 in the cross geometry. A focal spot of 12 μm vertically and 120 μm horizontally was thus obtained. Closing the primary slits located at 28 m from the source down to 10 μm reduced the horizontal spot size to 30 μm. SET#1 and SET#2 diamond plates were also installed aligned in tandem along the beam axis to achieve vertical focusing by a total of $N = 4$ single lenses all with radii $R = 200$ μm. In order to keep the same imaging distance, the energy was changed to 14.6 keV. A focal line width of $\sim$8.9 μm (FWHM) with a gain of 20 was measured.

The focusing properties of the CRL_2 SET#1 were also studied at an X-ray energy of 7.6 keV. The image distance L_2 was $\sim$4.3 m providing a source demagnification in the order of 13. In this case, the measured vertical width $\Delta = 3.1$ μm (FWHM) of the focal corresponded to an X-ray effective source size of 40 μm. It is worthwhile to note here that the angular resolution of our CRL is defined as Δ/L_2 and equals 0.72 μrad, and the experimental result $\Delta = 3.1$ μm means that the effective optical 'slope errors' of the lens are at least less than this value. Drawing the analogy to X-ray mirrors, where the r.m.s. slope of the figure error (Church & Takacs, 1995) is defined by $\Delta/2.36 \times 2L_2$, we obtain a value of 0.15 μrad for the lenses. This figure error is comparable with that of high-quality X-ray mirrors, while our approach to refractive optics can be achieved with far less cost and requires less surface perfection.

4. Conclusions

The present study demonstrated that laser micro-fabrication technology provides a straightforward method for the fabrication of single-crystal diamond refractive lenses with large acceptance (here 300 μm). The depth of the lenses can be increased by using thicker plates of single-crystal diamond which is commercially available grown by CVD to thicknesses to >1 mm; however, the difficulty of precise laser cutting increases rapidly with increasing plate thickness. Comparing polycrystalline materials (diamond or beryllium) with single-crystal diamond, single-crystal is preferred as it is free of the X-ray diffuse scattering from grain boundaries, voids, inclusions and other scattering centres which reduce the amount of radiation in the focal spot. Planar single-crystal diamond lenses with large depths are capable of withstanding extreme photon flux levels due to their extremely high thermal conductivity and shock resistance, low thermal expansion coefficient and high temperature stability: they therefore have a great future for free-electron lasers.

It is worth noting that one-dimensional beryllium lenses are easily available (http://www.rxoptics.de) and are already in use for white-beam collimation inside optics hutches (Theveneau *et al.*, 2013). However, they are almost at their application limit as front-end optical devices, particularly in view of the coming Phase-II ESRF upgrade program. From this point of view, diamond could be used on fourth-generation synchrotron sources for refractive lenses placed inside the beamline front-end as beam-conditioning optics for beam pre-focusing (*i.e.* collimation) or expanding (Snigirev *et al.*, 1997). In particular, such front-end optics will be in demand for the reduced emittance of future ultimate synchrotron storage rings, while a wide divergent beam will remain a requirement for a number of experimental techniques. However, we should note the lack of a well developed manufacturing technology for two-dimensional diamond lenses, which keeps beryllium as the immutable and fundamental material for two-dimensional refractive lenses.

Clearly, individual diamond plates with lenses of design such as those tested here can be stacked in tandem along the optical axis, forming long CRLs with a tunable number of lenses. This approach allows the use of different combinations of identical CRL-array diamond plates to achieve the total number of lenses required by the experiment.

We stress that due to the absence of a well developed diamond electronics industry as compared with that existing for silicon, RIE technologies are less well developed for diamond. Laser cutting could therefore be preferable for the fabrication of diamond lenses as compared with the development of deep RIE processes that also require the deposition of highly etch-selective mask material to obtain acceptable side-wall roughness and pattern fidelity. We believe the quality of the laser-cut surface profiles can be significantly improved by using recent ultraviolet femtosecond lasers and we are currently pursuing this with industrial partners in order to produce smoother surfaces with more precise geometric profiles that will increase the resolution, efficiency and gain that can be obtained with these CRLs. If successful, diamond refractive lenses can also be applied to hard X-ray microscopy and nano-probe techniques with high transparency and enhanced effective aperture [as $A_{\rm eff} \simeq (1/\beta)^{1/2}$, where the absorption coefficient β is low for diamond which is a very low-Z material].

The authors express their gratitude to the ID06 beamline staff for helping in performing these experiments, especially to C. Detlefs and P. Wattecamps, and Ch. Saulnier and Ch. Carrière of MicroUsinage Laser for discussions on optimizing the diamond laser cutting. Special thanks also go to Dr V. Ralchenko from GPI RAS. The work was supported in part by the Ministry of Education and Science of the Russian Federation (contract No. 14.Y26.31.0002 and 02.G25.31.0086).

References

Als-Nielsen, J., Freund, A. K., Grübel, G., Linderholm, J., Nielsen, M., del Rio, M. S. & Sellschop, J. P. F. (1994). *Nucl. Instrum. Methods Phys. Res. B*, **94**, 306–318.

Artemiev, A., Snigirev, A., Kohn, V., Snigireva, I., Artemiev, N., Grigoriev, M., Peredkov, S., Glikin, L., Levtonov, M., Kvardakov, V., Zabelin, A. & Maevskiy, A. (2006). *Rev. Sci. Instrum.* **77**, 063113.

Bello, I., Fung, M. K., Zhang, W. J., Lai, K. H., Wang, Y. M., Zhou, Z. F., Yu, R. K. W., Lee, C. S. & Lee, S. T. (2000). *Thin Solid Films*, **368**, 222–226.

Bjiorkman, H., Rangsten, P., Hollman, P. & Hjort, K. (1999). *Sens. Actuators A*, **73**, 20–29.
Church, E. L. & Takacs, P. Z. (1995). *Opt. Eng.* **34**, 353–360.
Fernandez, P. B., Graber, T., Lee, W. K., Mills, D. M., Rogers, C. S. & Assoufid, L. (1997). *Nucl. Instrum. Methods Phys. Res. A*, **400**, 476–483.
Fox, O. J. L., Alianelli, L., Malik, A. M., Pape, I., May, P. W. & Sawhney, K. J. S. (2014). *Opt. Express*, **22**, 7657–7668.
Grübel, G., Abernathy, D., Vignaud, G., Sanchez del Rio, M. & Freund, A. (1996). *Rev. Sci. Instrum.* **67**, 3349.
Isakovic, A. F., Stein, A., Warren, J. B., Narayanan, S., Sprung, M., Sandy, A. R. & Evans-Lutterodt, K. (2009). *J. Synchrotron Rad.* **16**, 8–13.
Khounsary, A. M., Smither, R. K., Davey, S. & Purohit, A. (1992). *Proc. SPIE*, **1739**, 628–642.
Kohn, V., Snigireva, I. & Snigirev, A. (2000). *Phys. Rev. Lett.* **85**, 2745–2748.
Kohn, V., Snigireva, I. & Snigirev, A. (2003). *Opt. Commun.* **216**, 247–260.
Lengeler, B., Schroer, C., Tümmler, J., Benner, B., Richwin, M., Snigirev, A., Snigireva, I. & Drakopoulos, M. (1999). *J. Synchrotron Rad.* **6**, 1153–1167.
Malik, A. M., Fox, O. J. L., Alianelli, L., Korsunsky, A. M., Stevens, R., Loader, I. M., Wilson, M. C., Pape, I., Sawhney, K. J. S. & May, P. W. (2013). *J. Micromech. Microeng.* **23**, 125018.
Nöhammer, B., Hoszowska, J., Freund, A. K. & David, C. (2003). *J. Synchrotron Rad.* **10**, 168–171.
Polikarpov, M., Snigireva, I. & Snigirev, A. (2014). *J. Synchrotron Rad.* **21**, 484–487.
Ralchenko, V. G., Khomich, A. V., Baranov, A. V., Vlasov, I. I. & Konov, V. I. (1999). *Phys. Status Solidi A*, **174**, 171–176.
Schroer, C. G. & Lengeler, B. (2005). *Phys. Rev. Lett.* **94**, 054802.
Shabel'nikov, L., Nazmov, V., Pantenburg, F. J., Mohr, J., Saile, V., Yunkin, V., Kouznetsov, S., Pindyurin, V. F., Snigireva, I. & Snigirev, A. A. (2002). *Proc. SPIE*, **4783**, 176–184.
Shu, D., Shvyd'ko, Y., Amann, J., Emma, P., Stoupin, S. & Quintana, J. (2013). *J. Phys. Conf. Ser.* **425**, 052004.
Snigirev, A., Filseth, B., Elleaume, P., Klocke, T., Kohn, V., Lengeler, B., Snigireva, I., Souvorov, A. & Tuemmler, J. (1997). *Proc. SPIE*, **3151**, 164–170.
Snigirev, A., Hustache, R., Duboc, P., Massonnat, J. Y., Claustre, L., Van Vaerenbergh, P., Snigireva, I., Grigoriev, M. & Yunkin, V. (2007). *Proc. SPIE*, **6705**, 670511.
Snigirev, A., Kohn, V., Snigireva, I. & Lengeler, B. (1996). *Nature (London)*, **384**, 49–51.
Snigirev, A., Snigireva, I., Grigoriev, M., Yunkin, V., Michiel, M. D., Vaughan, G., Kohn, V. & Kuznetsov, S. (2009). *J. Phys. Conf. Ser.* **186**, 012072.
Snigirev, A., Yunkin, V., Snigireva, I., Michiel, M. D., Drakopoulos, M., Kuznetsov, S., Shabelnikov, L., Grigoriev, M., Ralchenko, V., Sychov, I., Hoffmann, M. & Voges, E. (2002). *Proc. SPIE*, **4783**, 1–9.
Stoupin, S. *et al.* (2014). *J. Appl. Cryst.* **47**, 1329–1336.
Stoupin, S., Shvyd'ko, Y. V., Shu, D., Blank, V. D., Terentyev, S. A., Polyakov, S. N., Kuznetsov, M. S., Lemesh, I., Mundboth, K., Collins, S. P., Sutter, J. P. & Tolkiehn, M. (2013). *Opt. Express*, **21**, 30932–30946.
Theveneau, P. *et al.* (2013). *J. Phys. Conf. Ser.* **425**, 012001.
Tummler, J. (2000). Thesis, Rheinisch-Westfälische Technische Hochschule (RWTH) Aachen, Germany.
Vaughan, G. B. M., Wright, J. P., Bytchkov, A., Rossat, M., Gleyzolle, H., Snigireva, I. & Snigirev, A. (2011). *J. Synchrotron Rad.* **18**, 125–133.
Yabashi, M., Goto, S., Shimizu, Y., Tamasaku, K., Yamazaki, H., Yoda, Y., Suzuki, M., Ohishi, Y., Yamamoto, M. & Ishikawa, T. (2007). *AIP Conf. Proc.* **879**, 922–925.